

# Full nonuniversality of the symmetric 16-vertex model on the square lattice

Eva Pospíšilová, Roman Krčmár, Andrej Gendiar, and Ladislav Šamaj

*Institute of Physics, Slovak Academy of Sciences, Dúbravská cesta 9, 84511 Bratislava, Slovakia*

(Dated: February 6, 2022)

We consider the symmetric two-state 16-vertex model on the square lattice whose vertex weights are invariant under any permutation of adjacent edge states. The vertex-weight parameters are restricted to a critical manifold which is self-dual under the gauge transformation. The critical properties of the model are studied numerically by using the Corner Transfer Matrix Renormalization Group method. Accuracy of the method is tested on two exactly solvable cases: the Ising model and a specific version of the Baxter 8-vertex model in a zero field that belong to different universality classes. Numerical results show that the two exactly solvable cases are connected by a line of critical points with the polarization as the order parameter. There are numerical indications that critical exponents vary continuously along this line in such a way that the weak universality hypothesis is violated.

## I. INTRODUCTION

According to the universality hypothesis [1], critical exponents of a statistical system at the second-order phase transition do not depend on details of the corresponding Hamiltonian. Equivalently, the critical exponents depend only on the system's space dimensionality and the symmetry of microscopic degrees of freedom (say, the spins). The first violation of the universality hypothesis was observed in the Baxter's exact solution of the two-dimensional (2D) 8-vertex model on the square lattice in a zero electric field [2–4] whose critical exponents are functions of model's parameters. Suzuki [5] argued that the violation of universality in the 8-vertex model is due to an ambiguous identification of the deviation from the critical temperature. If taking, instead of the usual temperature difference  $|T_c - T|$ , the inverse correlation length  $\xi^{-1} \propto |T_c - T|^\nu$  (the critical exponent  $\nu$  is assumed to be the same for both limits  $T \rightarrow T_c^-$  and  $T \rightarrow T_c^+$ ) as the natural measure of the distance from the critical temperature, the renormalized thermal exponents  $\alpha/\nu$ ,  $\beta/\nu$  and  $\gamma/\nu$  become universal, i.e., independent of the model's parameters. The critical exponents defined just at the critical temperature, such as  $\delta = 1 + \frac{\gamma}{\beta}$  and  $\eta = 4/(\delta + 1)$ , stay constant when varying 8-vertex model's parameters. This phenomenon is known as weak universality. Weak universality was observed in many 2D systems, including the Ashkin-Teller model [6–8], absorbing phase transitions [9], the spin-1 Blume-Capel model [10], frustrated spin models [11, 12], percolation models [13], etc. There are few exceptions from models with continuously varying critical exponents which violate weak universality, such as micellar solutions [14], Ising spin glasses [15], itinerant composite magnetic materials [16, 17], etc.

To set up terminology, the full violation of universality means that the critical exponents vary continuously as functions of some model's parameter(s) in such a way that at least one of the renormalized thermal exponents  $\alpha/\nu$ ,  $\beta/\nu$ ,  $\gamma/\nu$  or  $\delta, \eta$  is nonconstant. We do not use the term nonuniversality for models which have

several regions in their parameter space belonging to different universality classes because the corresponding order parameters are defined differently.

The partition function of the “electric” 8-vertex model on the square lattice can be mapped onto the partition function of a “magnetic” Ising model on the dual (also square) lattice with the nearest-neighbor two-spin and four-spin interactions on a square plaquette [18, 19]. Baxter's exact solution of the zero-field 8-vertex model [2, 3] provides all magnetic critical exponents (exhibiting weak universality), but only one electric critical exponent (namely  $\beta_e$  which describes the temperature singularity of the spontaneous polarization). Recently two of us [20] argued that the critical exponents related to the divergence of the correlation length must coincide in both the magnetic and the electric models:  $\nu_e = \nu$ . Having two critical exponents at one's disposal, all remaining electric exponents can be derived by using scaling relations. The obtained analytic formulas for the electric critical exponents are in perfect agreement with numerical results obtained by the Corner Transfer Matrix Renormalization Group method [20]. It turns out that the model's variation of the electric critical exponents violates weak universality. Thus, despite the partition functions of the electric and magnetic models are equivalent, their critical properties are fundamentally different: while the magnetic critical exponents obey weak universality, the electric ones do not and therefore they are fully nonuniversal.

The partition function of a vertex model is invariant under gauge transformation of vertex weights [21, 22] which is a generalization of the weak-graph expansion [23] and the duality transformation. If a point in the parameter space of vertex weights is mappable onto itself by a nontrivial gauge transformation, that point belongs to the self-dual manifold where all critical points of second-order phase transitions lie.

The model under consideration in this paper is the symmetric two-state 16-vertex model on the square lattice whose vertex weights are isotropic, i.e., invariant under any permutation of the adjacent edge states. This model was introduced in Ref. [24] in connection

with the  $O(2)$  gauge transformation which preserves the permutation symmetry of vertex weights and its self-dual manifolds can be easily found. In a certain subspace of the vertex weights, the model can be mapped onto Ising spins in a field [25, 26]. The critical properties of the model were studied numerically by combining a series expansion on the lattice and the Coherent Anomaly method [27] in Ref. [28]. In spite of modest computer facilities and lack of efficient numerical methods at that time (almost 30 years ago), the numerical results indicate the full nonuniversality of the model. (For a recent survey of the general 16-vertex model with an enlargement of known mappings, see Ref. [29].)

The aim of this work is to revisit the study of the critical electric properties of the symmetric version of the 16-vertex model on the square lattice by using the Corner Transfer Matrix Renormalization Group (CTMRG) method [30–34]. The method is based on the density matrix renormalization [35–37] and the technique of the corner transfer matrices [3]. It has been applied to many 2D lattice models and provides very accurate results for critical points and exponents. The present work confirms with a high reliability that the symmetric 16-vertex on the square lattice is nonuniversal and violates the weak universality hypothesis.

The paper is organized as follows. The definition and basic facts about the model, including the gauge transformation of vertex weights, are given in Sec. II. Two exactly solvable cases are discussed: the Ising model and a specific version of the Baxter eight-vertex model in zero field. The CTMRG method is reviewed briefly in Sec. III. Numerical results for the critical temperatures and exponents are presented in IV. Sec. V brings a short recapitulation and concluding remarks.

## II. MODEL AND ITS EXACTLY SOLVABLE CASES

### A. Basic facts about the model

The general two-state vertex model on the square lattice of  $N$  ( $N \rightarrow \infty$ ) sites is defined as follows. Each lattice edge can be in one of two states. These states will be denoted either by  $\pm$  signs or by “dipole” arrows: the right/up oriented arrow corresponds to the (+) state, while the left/down arrow to the (−) state. With each vertex we associate the set of  $2^4$  possible Boltzmann weights  $w(s_1, s_2, s_3, s_4) = \exp[-\varepsilon(s_1, s_2, s_3, s_4)/T]$ . In units of  $k_B = 1$ , both the energy  $\varepsilon(s_1, s_2, s_3, s_4)$  and the temperature  $T$  are taken as dimensionless. For the symmetric version of the model, the vertex weights are invariant with respect to any permutation of state variables  $(s_1, s_2, s_3, s_4)$ . Let us denote by  $w_i = \exp(-\varepsilon_i/T)$  ( $i = 0, 1, \dots, 4$ ) the vertex weight with  $i$  incident edges in the (−) state and the remaining  $4 - i$  incident edges in the (+) state. Thus among the 16 possible configurations of vertex states there is 1

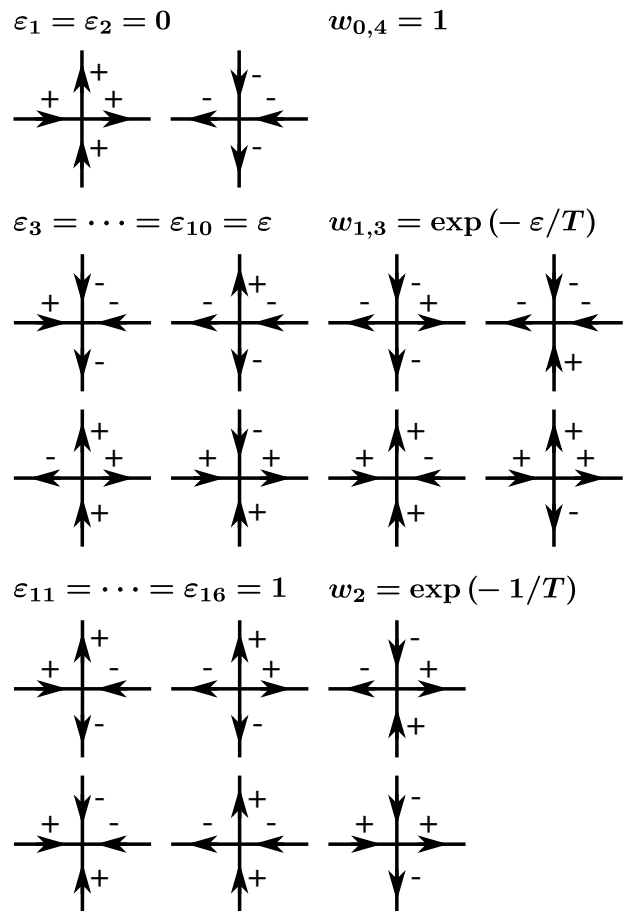


FIG. 1. Vertex weights of the symmetric 16-vertex model on the square lattice, invariant with respect to the flip of all adjacent edge states  $+ \leftrightarrow -$ .

configuration corresponding to each of the vertex weights  $w_0$  and  $w_4$ , 4 configurations corresponding to each of  $w_1$  and  $w_3$ , and 6 configurations corresponding to  $w_2$ , see Fig. 1.

Thermal equilibrium of the system is determined by the (dimensionless) free energy per site

$$-\frac{f(\{w\})}{T} = \lim_{N \rightarrow \infty} \frac{1}{N} \ln Z(\{w\}), \quad (1)$$

where

$$Z(\{w\}) = \sum_{\{s\}} \prod_{\text{vertex}} (\text{weights}), \quad (2)$$

is the partition function with the summation going over all possible edge configurations and the product being over all vertex weights on the lattice. The mean concentration  $c_i$  of the vertices with weight  $w_i$  is given by

$$c_i = -w_i \frac{\partial}{\partial w_i} \frac{f(\{w\})}{T} \quad (i = 0, \dots, 4). \quad (3)$$

The mean concentrations are constrained by the obvious normalization condition  $\sum_{i=0}^4 c_i = 1$ . The mean-value of the edge-state variable

$$P = \frac{1}{4} \sum_{i=0}^4 (4-2i)c_i \quad (4)$$

defines the polarization. When one applies an isotropic electric field  $E$  (with the same strength along either of the two axes), each arrow dipole  $s = \pm 1$  acquires the energy  $-Es$ . Since every dipole belongs to just two vertices, the vertex weights are modified to

$$w_i(E) = w_i \exp [E(2-i)/T]. \quad (5)$$

One can trivially extend the definitions of the vertex concentrations (3) and the polarization (4) to  $E \neq 0$ , with the corresponding notations  $c_i(E)$  and  $P(E)$ . Then the polarization susceptibility reads as

$$\chi = \lim_{E \rightarrow 0} \frac{\partial P(E)}{\partial E} = \frac{1}{2} \sum_{i,j=0}^4 (2-i)(2-j)\chi_{ij}, \quad (6)$$

where the elements

$$\chi_{ij} = -\frac{\partial}{\partial \epsilon_j} c_i(E=0) \quad (7)$$

form the tensor of generalized susceptibilities.

The partition function of the general two-state vertex model is invariant under the  $O(2)$  gauge transformation of the vertex weights [21, 22]. On the square lattice with the coordination number 4, the gauge transformation reads as

$$\begin{aligned} \tilde{w}(s_1, s_2, s_3, s_4) &= \sum_{s'_1, s'_2, s'_3, s'_4} V_{s_1 s'_1}(y) V_{s_2 s'_2}(y) V_{s_3 s'_3}(y) \\ &\quad \times V_{s_4 s'_4}(y) w(s'_1, s'_2, s'_3, s'_4). \end{aligned} \quad (8)$$

Here,  $V_{ss'}(y)$  are the elements of the matrix

$$\mathbf{V}(y) = \frac{1}{\sqrt{1+y^2}} \begin{pmatrix} 1 & y \\ y & -1 \end{pmatrix} \quad (9)$$

with rows (columns) indexed from up to down (left to right) as  $+$ ,  $-$  and a free (real) gauge parameter  $y$ . For the symmetric version of the vertex model, the gauge transformation keeps the permutation symmetry of the vertex weights [24], namely

$$\tilde{w}_i = \sum_{j=0}^4 W_{ij}(y) w_j \quad (i = 0, 1, \dots, 4), \quad (10)$$

$$W_{ij}(y) = \frac{1}{(1+y^2)^2} \sum_{k=0}^{\min(i,j)} \binom{i}{k} \binom{4-i}{j-k} (-1)^k y^{i+j-2k}. \quad (11)$$

The points in the vertex-weight parameter space, which can be mapped onto themselves by gauge transformation with a nontrivial (point-dependent) value of  $y \neq 0$ , form the so-called self-dual manifold. The self-dual manifold for the symmetric 16-vertex model is given by [24]

$$\begin{aligned} w_0^2 w_3 - w_1 w_4^2 - 3w_2(w_0 - w_4)(w_1 + w_3) \\ + (w_1 - w_3)[w_0 w_4 + 2(w_1 + w_3)^2] = 0. \end{aligned} \quad (12)$$

Its importance consists in the fact that all critical points of the second-order phase transitions are confined to this subspace of the vertex weights.

In this work, we restrict ourselves to the symmetric 16-vertex model whose vertex weights are invariant with respect to the flip of all adjacent edge states  $(+) \leftrightarrow (-)$ . The vertex weights are parametrized as follows

$$w_0 = w_4 = 1, \quad w_1 = w_3 = e^{-\epsilon/T}, \quad w_2 = e^{-1/T}, \quad (13)$$

see also Fig. 1, where the real energy parameter  $\epsilon \geq 0$ . It can be checked that this choice of vertex weights automatically satisfies the self-dual condition (12). Thus, for a fixed value of the energy  $\epsilon$ , there should exist a critical temperature  $T_c$  at which the second-order phase transition takes place. The order parameter is always the mean polarization  $P$ , see Eq. (4). In the disordered phase, for  $T > T_c$ , the state-flip symmetry of vertex weights implies the equality of mean vertex concentrations  $c_i = c_{4-i}$  ( $i = 0, 1$ ) and  $P$  vanishes. In the ordered phase, for  $T < T_c$ , the state-flip symmetry breaking causes that  $c_i \neq c_{4-i}$  and the spontaneous polarization  $P$  becomes nonzero. At  $T_c$ ,  $P$  is nonanalytic in  $T_c - T$ :

$$P \propto (T_c - T)^{\beta_e}, \quad T \rightarrow T_c^- \quad (14)$$

with  $\beta_e$  (the subscript e means ‘‘electric’’) being the critical exponent. If a small isotropic external electric field  $E$  is applied to the vertex system just at the critical temperature, the polarization behaves as

$$P(E) \propto E^{1/\delta_e}, \quad T = T_c, \quad (15)$$

where  $\delta_e$  is another critical exponent. Close to the critical point, the polarization susceptibility (6) exhibits a singularity of type

$$\chi \propto \frac{1}{|T_c - T|^{\gamma_e}}, \quad (16)$$

where the critical exponent  $\gamma_e$  is assumed to be the same for both limits  $T \rightarrow T_c^-$  and  $T \rightarrow T_c^+$ . The pair arrow-arrow correlation function exhibits the large-distance behavior

$$G_e(r) \propto \frac{1}{r^{\eta_e}} \exp(-r/\xi), \quad r \rightarrow \infty. \quad (17)$$

Approaching the critical point, the correlation length  $\xi$

diverges as

$$\xi \propto \frac{1}{|T_c - T|^{\nu_e}}. \quad (18)$$

The divergence of  $\xi$  at  $T = T_c$  reflects the fact that the short-range (exponential) decay changes into the long-range (inverse power-law) decay at  $T = T_c$ , which is characterized by the critical exponent  $\eta_e$ .

Having at one's disposal the two critical exponents  $\beta_e$  and  $\delta_e$ , the remaining ones (considered in this work) can be calculated by the 2D scaling relations [3]:

$$\gamma_e = \beta_e (\delta_e - 1), \quad (19a)$$

$$\nu_e = \frac{1}{2} \beta_e (\delta_e + 1), \quad (19b)$$

$$\eta_e = \frac{4}{\delta_e + 1}. \quad (19c)$$

### B. Ising point

The symmetric 16-vertex model can be mapped onto the Ising model on the square lattice under the vertex-weight constraint [25, 26]

$$w_0 w_2 w_4 - w_0 w_3^2 - w_1^2 w_4 + 2 w_1 w_2 w_3 - w_2^3 = 0. \quad (20)$$

For the state-flip symmetry of the vertex weights (13), this equation takes the form

$$1 + e^{1/T} = 2e^{2(1-\varepsilon)/T}. \quad (21)$$

As concerns the parameters of the Ising model for the state-flip symmetry, the external magnetic field acting on spins  $H = 0$  and the (dimensionless) coupling  $J$  between the nearest-neighbor spins is given by

$$J = \frac{1}{2} \ln \left( \frac{w_1}{w_2} \right) = \frac{1 - \varepsilon}{2T}. \quad (22)$$

The known critical value of the Ising coupling reads [3]

$$J_c = \frac{1}{2} \ln \left( 1 + \sqrt{2} \right). \quad (23)$$

Consequently, Eqs. (21) and (22) imply the following critical parameters of the symmetric 16-vertex model:

$$\varepsilon^{(1)} = 1 - \frac{\ln(1 + \sqrt{2})}{\ln(5 + 4\sqrt{2})} = 0.627516\dots, \quad (24)$$

$$T_c^{(1)} = \frac{1}{\ln(5 + 4\sqrt{2})} = 0.422618\dots \quad (25)$$

In contrast to standard mappings of models on dual lattices, the mapping between the symmetric 16-vertex and the Ising models is made on the *same* square lattice [25, 26]. The relation between the polarization of the symmetric 16-vertex model and the magnetization of the equivalent Ising system can be derived by using the

technique presented in Ref. [38]. This relation is linear and, therefore, the critical exponents of the symmetric 16-vertex model are identical to the ones of the Ising model. The Ising critical exponents are summarized in Table I.

exponent	$\beta_e$	$\delta_e$	$\gamma_e$	$\nu_e$	$\eta_e$
$\varepsilon^{(1)} \approx 0.6275$	1/8	15	7/4	1	1/4
$\varepsilon \rightarrow \infty$	1/8	11	5/4	3/4	1/3

TABLE I. List of electric critical exponents for the symmetric 16-vertex model at the exactly solvable Ising and the Baxter 8-vertex points.

### C. 8-vertex point

When  $\varepsilon \rightarrow \infty$ , the vertex weights  $w_1$  and  $w_3$ , corresponding in Fig. 1 to configurations with odd numbers of (+), or equivalently (-), edge states, vanish. The consequent Baxter's 8-vertex model has vertex-weight parameters  $a = w_0 = w_4 = 1$  and  $b = c = d = w_2 = \exp(-1/T)$  [3]. The vertex system exhibits the ferroelectric-A phase for  $a > b + c + d$ . The second-order transition between the ferroelectric-A and disordered phases takes place at

$$a_c = b_c + c_c + d_c, \quad T_c = \frac{1}{\ln 3} = 0.910239\dots \quad (26)$$

Introducing the auxiliary parameter

$$\mu = 2 \arctan \left( \sqrt{\frac{a_c b_c}{c_c d_c}} \right) = \frac{2\pi}{3}, \quad (27)$$

according to Ref. [20] the electric critical exponents are given by

$$\begin{aligned} \beta_e &= \frac{\pi - \mu}{4\mu} = \frac{1}{8}, \\ \delta_e &= \frac{3\pi + \mu}{\pi - \mu} = 11, \\ \gamma_e &= \frac{\pi + \mu}{2\mu} = \frac{5}{4}, \\ \nu_e &= \frac{\pi}{2\mu} = \frac{3}{4}, \\ \eta_e &= 1 - \frac{\mu}{\pi} = \frac{1}{3}. \end{aligned} \quad (28)$$

These critical exponents are listed in Table I.

## III. NUMERICAL METHOD

The CTMRG method [30–32] is based on Baxter's technique of corner transfer matrices [3]. Each quadrant

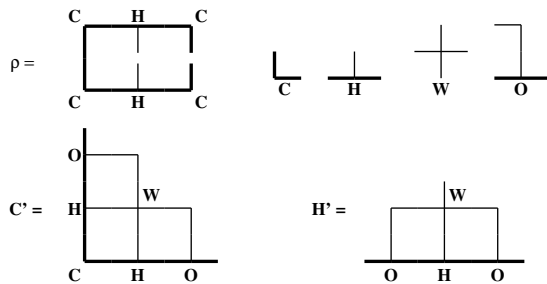


FIG. 2. The CTMRG renormalization process. The density matrix  $\rho$  is composed of four transfer matrices  $C$ . The expansion process of the corner transfer matrix  $C \rightarrow C' = O^\dagger H W C H O$  and the half-row transfer matrix  $H \rightarrow H' = O^\dagger H W O$  from the previous iteration RG Step, see the text.

of the square lattice with size  $L \times L$  is represented by the corner transfer matrix  $C$ . The reduced density matrix is defined by  $\rho = \text{Tr}' C^4$  (where the partial trace  $\text{Tr}'$  is taken), so that the partition function  $Z = \text{Tr} \rho$ , see Fig. 2. The number of degrees of freedom grows exponentially with  $L$  and the density matrix is used in the process of their reduction. Namely, degrees of freedom are iteratively projected to the space generated by the eigenvectors of the reduced density matrix  $\rho$  with the largest eigenvalues. The projector on this reduced space of dimension  $m$  is denoted by  $O$ ; the larger the truncation parameter  $m$  is taken, the better precision of the results is attained. In each iteration the linear system size is expanded from  $2L$  to  $2L + 2$  via the inclusion of the Boltzmann weight  $W$  of the basic vertex (see Fig. 1). The expansion process transforms the corner transfer matrix  $C$  to  $C'$  and the half-row transfer matrix  $H$  to  $H'$  in the way represented schematically in Fig. 2. The thin (thick) lines represent renormalized (multi-) arrow variables obtained after the renormalization. The fixed boundary conditions are imposed, i.e., the state (—) is fixed on the boundary arrows only. This choice ensures a quicker convergence of the method in the thermodynamic limit.

#### IV. NUMERICAL RESULTS

According to Eq. (14), the critical temperature  $T_c$  is the lowest temperature at which  $P = 0$  or, equivalently, the highest temperature at which  $P \neq 0$ . Based on comparison with the known values of the Ising (25) and Baxter's (26) critical temperatures, the error in estimation of  $T_c(\varepsilon)$  is of order  $10^{-4}$  for all values of  $\varepsilon$ . The error is even smaller (of order  $10^{-5}$ ) when fitting data for the spontaneous polarization close to the critical point according to (14). Numerical results for the  $\varepsilon$ -dependence of the critical temperature are shown in Fig. 3. We see that  $T_c(\varepsilon)$  is only weakly affected by dimension of the truncated space  $m = 100$  and  $m = 200$ , which means that our results reached the sufficient accuracy.

The inset of Fig. 3 documents the log-log plot of the

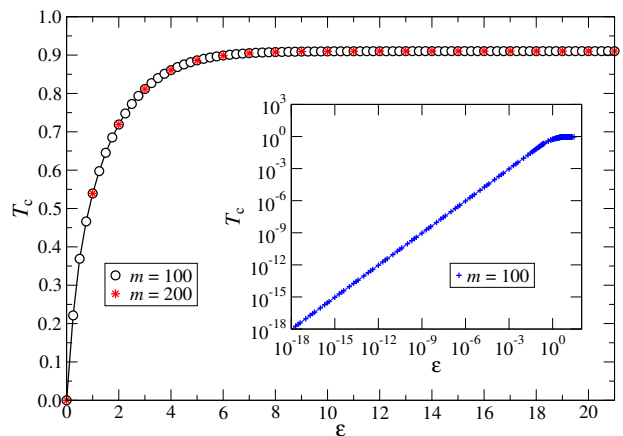


FIG. 3. The  $\varepsilon$ -dependence of the critical temperature  $T_c$  of the symmetric 16-vertex model, for dimension of the truncated space  $m = 100$  (open circles) and  $m = 200$  (open circles with stars). The inset shows a linear dependence of  $T_c(\varepsilon)$  for small values of  $\varepsilon$ .

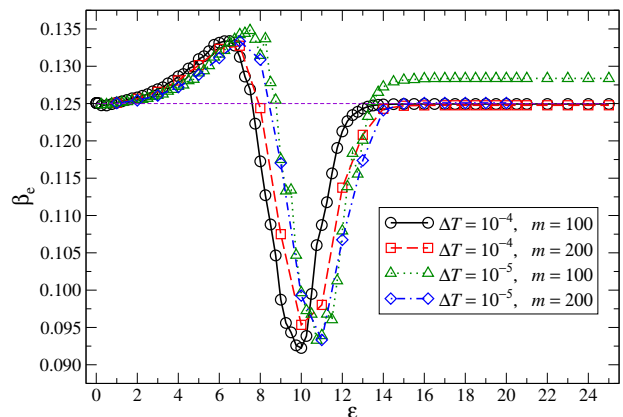


FIG. 4. The  $\varepsilon$ -dependence of the critical exponent  $\beta_e$  for the symmetric 16-vertex model with the temperature steps  $\Delta T = 10^{-4}$  and  $10^{-5}$  and dimensions of the truncated space  $m = 100$  and  $m = 200$ .

small- $\varepsilon$  behavior of  $T_c(\varepsilon)$ . The power-law least-square fitting at low  $\varepsilon < 10^{-8}$  yields

$$T_c(\varepsilon) = -6.6 \times 10^{-18} + 0.954(5)\varepsilon^{0.9998(3)}, \quad (29)$$

where the absolute term is on the accuracy border of the computer (the machine precision). We conclude that in the limit of small  $\varepsilon$  the critical temperature converges to zero linearly. On the other hand, as  $\varepsilon$  increases, the critical temperature saturates quickly to the value 0.91024 which is close to the asymptotic  $\varepsilon \rightarrow \infty$  analytic result (26) of the 8-vertex model.

The critical exponent  $\beta_e$  is expected to interpolate between the same values  $1/8$  at small and large  $\varepsilon$ . It is calculated by fitting the polarization data according to formula (14). With  $T_c$  fixed in the previous calculation,

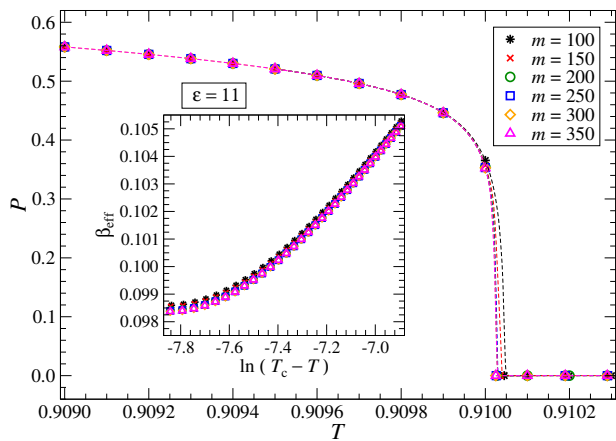


FIG. 5. The polarization (the order parameter)  $P$  as a function of temperature  $T$  calculated at  $\varepsilon = 11$  and for various numbers of the states reduction  $m$  ranging from 100 to 350. The inset shows the dependence of the effective critical exponent  $\beta_{\text{eff}}$  on the logarithmic distance of the temperature from the critical temperature  $T_c$ ; as  $T$  approaches  $T_c$  from below,  $\beta_{\text{eff}}(T \rightarrow T_c) \rightarrow \beta_e$ .

we have selected a series of temperatures below the threshold value  $T_c - 0.0002$  with a temperature spacing (discretization step)  $\Delta T$  at which the polarization is evaluated. For each value of  $\varepsilon$ , we have generated 6 polarization values with  $\Delta T = 10^{-4}$  and 30 polarization values with  $\Delta T = 10^{-5}$  if taking dimension of the truncated space  $m = 100$  and  $m = 200$ . The corresponding  $\varepsilon$ -dependences of the critical exponent  $\beta_e$  within the range of  $\varepsilon \in [0, 25]$ , are pictured in Fig. 4. We see that the too small value of the temperature step  $\Delta T = 10^{-5}$  and  $m = 100$  (triangles) leads in the region of large  $\varepsilon$  incorrectly to  $\beta_e > 1/8$ . If increasing the accuracy to  $m = 200$  (diamonds), data converge to the correct value  $\beta_e = 1/8$  at large  $\varepsilon$ . On the other hand, for a larger temperature step  $\Delta T = 10^{-4}$ , both  $m = 100$  (circles) and  $m = 200$  (squares) data are consistent with  $\beta_e = 1/8$  at large  $\varepsilon$ . We refer to the parameters  $\Delta T = 10^{-4}$  and  $m = 200$  as the optimal ones. The choice of these optimal parameters correctly reproduces the exact results for the Ising  $\varepsilon^{(1)} \approx 0.627516\dots$  and the 8-vertex  $\varepsilon \rightarrow \infty$  models and, therefore, it is expected to be adequate also in the transition region between the two solvable cases. The above-discussed cases are presented in Fig. 4 to judge the relative accuracy of the relevant data in the transition region of  $\varepsilon$  values. In the interval of  $\varepsilon \lesssim 2$  containing the Ising point  $\varepsilon = 0.627516\dots$ , the exponent is roughly constant  $\beta_e = 1/8$ . In the transition region  $2 \lesssim \varepsilon \lesssim 14$ ,  $\beta_e$  varies nonmonotonously as a function of  $\varepsilon$ . For  $\varepsilon \gtrsim 14$ , the exponent  $\beta_e$  is again constant and acquires its Baxter's ( $\varepsilon \rightarrow \infty$ ) value  $\beta_e = 1/8$ , as it should be.

To document the accuracy of the CTMRG method, we present in Fig. 5 the evaluation of the critical exponent  $\beta_e$  for the energy  $\varepsilon = 11$  which lies in the transition

region. The truncation orders  $m$  range from 100 to 350 and the optimal  $\Delta T = 10^{-4}$  is chosen. We define the effective exponent  $\beta_{\text{eff}}$  as follows

$$P(T) \propto (T_c - T)^{\beta_{\text{eff}}(T)}, \quad \text{for } 0 \ll T \leq T_c, \quad (30)$$

where the prefactor does not depend on the temperature. As  $T$  approaches  $T_c$  from below, the exponent  $\beta_{\text{eff}}(T)$  converges to the electric exponent  $\beta_e$  we are looking for:

$$\lim_{T \rightarrow T_c} \beta_{\text{eff}}(T) = \lim_{T \rightarrow T_c} \frac{\partial \ln P(T)}{\partial \ln(T_c - T)} = \beta_e. \quad (31)$$

As seen in the inset of Fig. 5, the data for  $\beta_{\text{eff}}$  as the function of the logarithmic distance of the temperature from  $T_c$  get converged starting from  $m = 200$ . The plot of  $\beta_{\text{eff}}$  is almost constant for  $\ln(T_c - T) < -7.8$ ; with regard to the fine scale on the  $\beta_{\text{eff}}$ -axis this fact permits an accurate determination of  $\beta_e$ . Since the accuracy of the CTMRG method is superior to standard numerical approaches like Monte Carlo simulations, the continuous variation of  $\beta_e$  in Fig. 4, ranging in the large interval  $2 \lesssim \varepsilon \lesssim 14$ , exhibits a relatively large amplitude exceeding by orders the error bars in the exponent determination by the present technique. In the same manner, we have analyzed the critical exponents investigated in the remaining part of the paper.

As seen in Table I, the critical exponent  $\delta_e$  is expected to interpolate between the values 15 at small  $\varepsilon$  and 11 at large  $\varepsilon$ . It is calculated by fitting the polarization data at the critical temperature  $T_c$  according to the relation (15) which can be rewritten as

$$\delta_e = \lim_{E \rightarrow 0} \left( \frac{\partial \ln P}{\partial \ln E} \right)^{-1}. \quad (32)$$

This formula has to be considered for a very small value of field  $E$ , but not too small to avoid numerical errors due to the critical state of the vertex system. The obtained data for  $E = 10^{-5}$  and  $2.5 \times 10^{-5}$  are presented in Fig. 6, within the range of  $\varepsilon \in [0, 18]$ . Data for  $E = 10^{-5}$ , evaluated at approximation orders  $m = 100$  (circles) and  $m = 200$  (squares), converge below the anticipated value 11. On the other hand, numerical data for the optimal field  $E = 2.5 \times 10^{-5}$  evaluated at approximation order  $m = 100$  (triangles) lie close to the previous data for  $E = 10^{-5}$  with  $m = 200$  in the region  $0 \lesssim \varepsilon \lesssim 12$  and tend to the correct value 11 for large values of  $\varepsilon$ .

The critical exponent  $\gamma_e$  is expected to interpolate between  $7/4$  at small  $\varepsilon$  and  $5/4$  at large values of  $\varepsilon$ . This exponent is calculated by fitting the susceptibility data according to the formula (16). The fitting is performed in the region  $T > T_c$  with the susceptibility functional values from the interval  $\chi \in [10000, 50000]$ . Within the range of  $\varepsilon \in [0, 18]$ , the obtained  $m = 100$  data are represented by triangles in Fig. 7. Data tend for small and large values of  $\varepsilon$  correctly to  $7/4$  and  $5/4$ , respectively. Because the fits of the singular formula (16) are accompanied by relatively large errors, we have

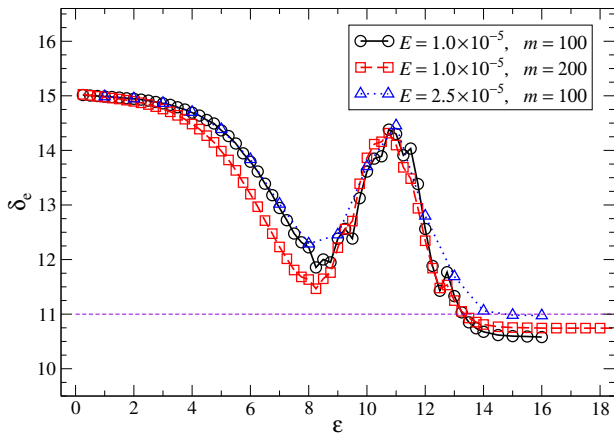


FIG. 6. The  $\varepsilon$ -dependence of the critical exponent  $\delta_e$  for the symmetric 16-vertex model. Data are generated for the electric field  $E = 10^{-5}$  at approximation orders  $m = 100$  (circles) and  $m = 200$  (squares), and the optimal  $E = 2.5 \times 10^{-5}$  at  $m = 100$  (triangles).

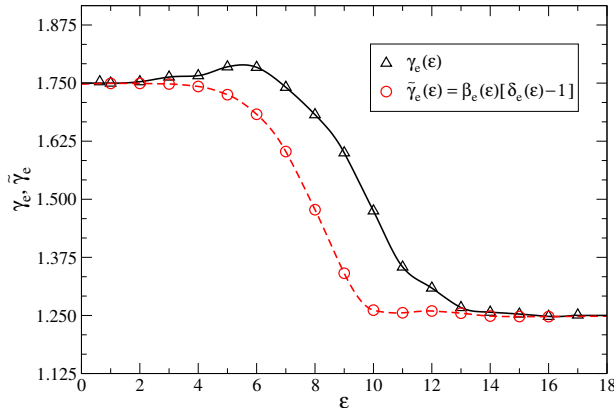


FIG. 7. The  $\varepsilon$ -dependence of the critical exponent  $\gamma_e$  for the symmetric 16-vertex model. Data are generated from fitting of the formula (16), in the region  $T > T_c$  and the susceptibility values  $\chi \in [10000, 50000]$  calculated with dimension of the truncated space  $m = 100$  (triangles). The exponent  $\tilde{\gamma}_e$ , calculated by inserting the previous data for  $\beta_e$  and  $\delta_e$  into the scaling relation (19a), is represented by circles.

calculated alternatively  $\tilde{\gamma}_e$  by inserting the previous data for  $\beta_e$  and  $\delta_e$  into the scaling relation (19a). Hereinafter, we adopt convention that an exponent deduced by using scaling relations will be denoted by a tilde on its top. The data for  $\tilde{\gamma}_e$  are represented in Fig. 7 by circles. Note that the plot exhibits a monotonous decay.

The critical exponents  $\tilde{\nu}_e$  and  $\tilde{\eta}_e$ , calculated by inserting the previous data for  $\beta_e$  ( $\Delta T = 10^{-4}$  and  $m = 200$ , squares in Fig. 4) and  $\delta_e$  ( $E = 2.5 \times 10^{-5}$  and  $m = 100$ , triangles in Fig. 6) into the scaling relations (19b) and (19c), respectively, are represented as functions of  $\varepsilon$  in Fig. 8 by triangles and circles. Both plots exhibit nonmonotonous behavior. The exponent  $\tilde{\nu}_e$  interpolates

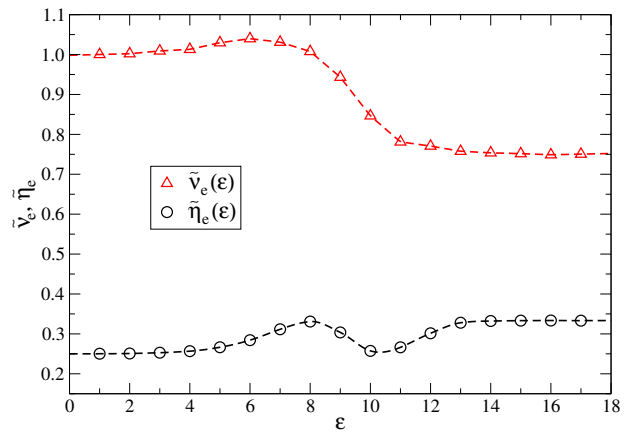


FIG. 8. The critical exponents  $\tilde{\nu}_e$  (triangles) and  $\tilde{\eta}_e$  (circles), calculated by inserting the previous data for  $\beta_e$  ( $\Delta T = 10^{-4}$  and  $m = 200$ ) and  $\delta_e$  ( $E = 2.5 \times 10^{-5}$  and  $m = 100$ ) into the second and third of scaling relations (19b), respectively, as functions of  $\varepsilon \in [0, 18]$ .

correctly between 1 at small  $\varepsilon$  and  $3/4$  at large  $\varepsilon$  and  $\tilde{\eta}_e$  interpolates correctly between  $1/4$  at small  $\varepsilon$  and  $1/3$  at large  $\varepsilon$ .

The accuracy of the CTMRG method is superior to that of the standard numerical transfer matrix and Monte Carlo methods. The crucial feature of the present method is the extremely small error of order  $10^{-4} - 10^{-5}$  in the determination of the critical temperature  $T_c(\varepsilon)$ , whereas the error decreases to the machine precision ( $10^{-16}$ ) off  $T_c(\varepsilon)$ . Having the precise value of the critical temperature, the fitting of the critical exponents  $\beta_e$  by using (14) and  $\gamma_e$  by using (32) is very accurate. For the purpose of benchmarking, we employ a numerical method, the Higher-Order Tensor Renormalization Group (HOTRG) [39], in order to provide an independent comparison with the CTMRG. We chose the HOTRG method for its numerical reliability and high accuracy with respect to the Monte Carlo simulations. Having defined the absolute errors  $\mathcal{E}_{T_c}(\varepsilon) = |T_c^{\text{HOTRG}}(\varepsilon) - T_c^{\text{CTMRG}}(\varepsilon)|$  and  $\mathcal{E}_{\beta_e}(\varepsilon) = |\beta_e^{\text{HOTRG}}(\varepsilon) - \beta_e^{\text{CTMRG}}(\varepsilon)|$ , we confirmed an excellent agreement between the CTMRG and HOTRG methods. In particular, we evaluated the errors at four points  $\varepsilon = 9, 10, 11, 12$  of the transition region, where the exponents change rapidly, see Tab. II.

Our first aim was to confirm that there is a line of critical points connecting the two exactly solvable Ising  $\varepsilon^{(1)} \approx 0.6275$  and 8-vertex  $\varepsilon \rightarrow \infty$  points which belong to two different universality classes. The order parameter, namely the polarization (4), is unique for all values of  $\varepsilon \geq 0$ . The next question was whether the critical exponents are changing along the line continuously, or they are constant in the regions of small and large  $\varepsilon$  with a discontinuous change at intermediate values of  $\varepsilon$ . As seen in Figs. 4 and 6, the variation of the two crucial critical exponents  $\beta_e$  and  $\gamma_e$  is considerable and takes

$\varepsilon$	$\mathcal{E}_{T_c}(\varepsilon)$	$\mathcal{E}_{\beta_e}(\varepsilon)$
9	$5 \times 10^{-6}$	$6.8 \times 10^{-4}$
10	$3 \times 10^{-6}$	$7.8 \times 10^{-4}$
11	$2 \times 10^{-6}$	$2.8 \times 10^{-4}$
12	$2 \times 10^{-6}$	$1.9 \times 10^{-3}$

TABLE II. The absolute errors of the results for the critical temperatures  $T_c$  and the critical exponents  $\beta_e$  obtained by using the CTMRG and HOTRG methods.

place on a relatively large interval  $2 \lesssim \varepsilon \lesssim 14$ . With regard to the high accuracy of the CTMRG method, this fact supports the scenario of a continuous change of the critical exponents along the line. The same arguments hold as to the variation of the critical exponents  $\gamma(\varepsilon)$  in Fig. 7 and  $\eta(\varepsilon)$  in Fig. 8, but the variation of  $\nu_e$  in Fig. 8 permits the scenario of two universality classes only.

To judge the validity of the hypothesis of weak universality, it is sufficient to test the thermal renormalized exponents  $\beta_e/\nu_e$ ,  $\gamma_e/\nu_e$  and the exponents  $\delta_e, \eta_e$ , which are independent of  $\varepsilon$  if weak universality applies, at the two exactly solvable points. In particular, from Table I we have

$$\frac{\beta_e}{\nu_e} = \begin{cases} \frac{1}{8} & \varepsilon^{(1)} \approx 0.6275, \\ \frac{1}{6} & \varepsilon \rightarrow \infty, \end{cases} \quad (33)$$

$$\frac{\gamma_e}{\nu_e} = \begin{cases} \frac{7}{4} & \varepsilon^{(1)} \approx 0.6275, \\ \frac{5}{3} & \varepsilon \rightarrow \infty, \end{cases} \quad (34)$$

$$\delta_e = \begin{cases} 15 & \varepsilon^{(1)} \approx 0.6275, \\ 11 & \varepsilon \rightarrow \infty, \end{cases} \quad (35)$$

$$\eta_e = \begin{cases} \frac{1}{4} & \varepsilon^{(1)} \approx 0.6275, \\ \frac{1}{3} & \varepsilon \rightarrow \infty. \end{cases} \quad (36)$$

The fact that  $\gamma_e/\nu_e$  and  $\delta_e, \eta_e$  are different at the two exactly solvable cases supports the full nonuniversality of the symmetric 16-vertex model on the square lattice.

## V. CONCLUSION

The system under consideration was the symmetric two-state 16-vertex model on the square lattice.

Its vertex weights, which are invariant under any permutation of adjacent edge states, are considered to be symmetric with respect to the flip of all adjacent edge states  $(+) \leftrightarrow (-)$  (see Fig. 1). Such vertex weights automatically lie on the self-dual manifold of the gauge transformation (12), i.e., the subspace of the parameter space which contains all the critical points. The order parameter is the mean polarization  $P$ , see Eq. (4). The parametrization of vertex weights (13) contains two positive parameters, the temperature  $T$  and the energy  $\varepsilon$ . The two exactly solvable cases, namely the Ising model and the specific version of Baxter's 8-vertex model correspond to  $\varepsilon^{(1)} \approx 0.6275$  and  $\varepsilon \rightarrow \infty$ , respectively. To study the critical properties of the model, we have applied the very accurate CTMRG method. The dependence of the critical temperature  $T_c$  on  $\varepsilon$  is pictured in Fig. 3. The fit of the plot in the region of small  $\varepsilon$  (see the inset) indicates the linear dependence with  $T_c$  going to 0 as  $\varepsilon \rightarrow 0$ . The plot of the critical exponent  $\beta_e$  versus  $\varepsilon$ , calculated with optimal parameters of the temperature step  $\Delta T = 10^{-4}$  and dimension of the reduced space  $m = 200$ , is represented by squares in Fig. 4. The critical exponent  $\delta_e(\varepsilon)$  is calculated with optimal parameters of the electric field  $E = 2.5 \times 10^{-5}$  and  $m = 100$ , see triangles in Fig. 6. The plots of the exponent  $\gamma_e$  versus  $\varepsilon$  are evaluated "from first principles" (triangles) and by using the scaling relation (19a) (circles) in Fig. 7. The dependence of the critical exponents  $\nu_e$  and  $\eta_e$  on  $\varepsilon$ , evaluated by (19b) and (19c), are presented in Fig. 8. All the critical exponents interpolate correctly between their known values at the two solvable cases  $\varepsilon^{(1)} \approx 0.6275$  and  $\varepsilon \rightarrow \infty$ . The continuous variation of the critical exponents with the model parameter  $\varepsilon$  is such that the weak universality hypothesis is violated.

## ACKNOWLEDGMENTS

The support received from the project EXSES APVV-16-0186 and VEGA Grants Nos. 2/0003/18 and 2/0123/19 is acknowledged.

- 
- [1] R. B. Griffiths, Phys. Rev. Lett. **24**, 1479 (1970).
  - [2] R. J. Baxter, Phys. Rev. Lett. **26**, 832 (1971).
  - [3] R. J. Baxter, *Exactly Solved Models in Statistical Mechanics*, (Academic Press, London, 1982).
  - [4] L. Šamaj and Z. Bajnok, *Introduction to the Statistical Physics of Integrable Many-body Systems* (Cambridge University Press, Cambridge, 2013).
  - [5] M. Suzuki, Prog. Theor. Phys. **51**, 1992 (1974).
  - [6] J. Ashkin and E. Teller, Phys. Rev. **64**, 178 (1943).
  - [7] L. P. Kadanoff, Phys. Rev. Lett. **39**, 903 (1977).
  - [8] A. B. Zisook, J. Phys. A: Math. Gen. **13**, 2451 (1980).
  - [9] J. D. Noh and H. Park, Phys. Rev. E **69**, 016122 (2004).
  - [10] A. Malakis, A. N. Berker, I. A. Hadjiagapiou, and N. G. Fytas, Phys. Rev. E **79**, 011125 (2009).
  - [11] S. L. A. de Queiroz, Phys. Rev. E **84**, 031132 (2011).



- [12] S. Jin, A. Sen, and A. W. Sandvik, *Phys. Rev. Lett.* **108**, 045702 (2012).
- [13] R. F. S. Andrade and H. J. Herrmann, *Phys. Rev. E* **88**, 042122 (2013).
- [14] M. Corti, V. Degiorgio, and M. Zulauf, *Phys. Rev. Lett.* **48**, 1617 (1982).
- [15] L. Bernardi and I. A. Campbell, *Phys. Rev. B* **52**, 12501 (1995).
- [16] D. Fuchs et al. *Phys. Rev. B* **89**, 174405 (2014).
- [17] N. Khan, P. Sarkar, A. Midya, P. Mandal, and P. K. Mohanty, *Sci. Rep.* **7**, 45004 (2017).
- [18] F. Y. Wu, *Phys. Rev. B* **4**, 2312 (1971).
- [19] L. P. Kadanoff and F. J. Wegner, *Phys. Rev. B* **4**, 3989 (1971).
- [20] R. Krčmár and L. Šamaj, *Phys. Rev. E* **97**, 012108 (2018).
- [21] F. J. Wegner, *Physica* **68**, 570 (1973).
- [22] A. Gaaff and J. Hijmans, *Physica A* **80**, 149 (1975).
- [23] J. F. Nagle, *J. Math. Phys.* **9**, 1007 (1968).
- [24] X. N. Wu and F. Y. Wu, *J. Phys. A: Math. Gen.* **22**, L55 (1989).
- [25] L. Šamaj and M. Kolesík, *Mod. Phys. Lett. B* **5**, 1075 (1991).
- [26] L. Šamaj and M. Kolesík, *Physica A* **182**, 455 (1992).
- [27] M. Suzuki, *J. Phys. Soc. Jpn.* **55**, 4205 (1986).
- [28] M. Kolesík and L. Šamaj, *J. Stat. Phys.* **72**, 1203 (1993).
- [29] M. Assis, *J. Phys. A: Math. Theor.* **50**, 395001 (2017).
- [30] T. Nishino and K. Okunishi, *J. Phys. Soc. Jpn.* **65**, 891 (1996).
- [31] T. Nishino and K. Okunishi, *J. Phys. Soc. Jpn.* **66**, 3040 (1997).
- [32] K. Ueda, R. Otani, Y. Nishio, A. Gendiar, and T. Nishino, *J. Phys. Soc. Jpn.* **74**, 1871 (2005).
- [33] R. Krčmár and L. Šamaj, *Europhys. Lett.* **115**, 56001 (2016).
- [34] J. Genzor, T. Nishino, and A. Gendiar, *Acta Phys. Slov.* **67**, 85 (2017).
- [35] S. R. White, *Phys. Rev. Lett.* **69**, 2863 (1992).
- [36] S. R. White, *Phys. Rev. B* **48**, 10345 (1993).
- [37] U. Schollwöck, *Rev. Mod. Phys.* **77**, 259 (2005).
- [38] M. Kolesík and L. Šamaj, *Physica A* **179**, 145 (1991).
- [39] Z. Y. Xie, J. Chen, M. P. Qin, J. W. Zhu, L. P. Yang, and T. Xiang, *Phys. Rev. B* **86**, 045139 (2012).